Predicting failure load of a non-crimp fabric composite by means of a 3D finite element model including progressive damage

Authors: Luis Miguel Ferreira [a,b] (corresponding author), Enrique Graciani [a], Federico París [a]

Affiliation:

a. Grupo de Elasticidad y Resistencia de Materiales, Escuela Técnica Superior de Ingeniería, Universidad de Sevilla.
b. Abu Dhabi Men's College, Higher Colleges of Technology.

Address:

a. Grupo de Elasticidad y Resistencia de Materiales. Escuela Técnica Superior de Ingeniería. Camino de los Descubrimientos s/n. 41092 Sevilla, España. Phone: +34 954 487 300. Fax: +34 954 461 637.
b. Abu Dhabi Men's College, 25035 Abu Dhabi, United Arab Emirates.

Email: lferreira@hct.ac.ae (Luis Miguel Ferreira), egraciani@us.es (Enrique Graciani), fparis@us.es (Federico París).

Abstract

A mesoscopic scale 3D finite element model of its representative unit cell is used to study the progressive damage of a $[0,90]_n$ non-crimp fabric laminate under compressive loading. The tows of the unit cell have been generated with a straight finite element mesh, and the out-of-plane fibre crimp has been incorporated into the model by defining the mechanical properties of each element according to the actual direction of the fibres. The material properties degradation (MPDG) method has been used to study the damage evolution. Non-interactive criteria (Maximum Stress and Maximum Strain), and interactive criteria (Hashin and Puck), associated with failure modes, have been employed to determine the onset of the material degradation at the fibre tows. The progressive damage throughout the mesoscopic unit cell, from the load at which damage is initiated, until the load at which the failure of the laminate is predicted, has been analysed. The mechanism responsible for the failure of the laminate has also been identified. The numerical predictions of the failure stress and failure strain, for the considered failure criteria, are discussed and compared with experimental data obtained from direct compression tests on biaxial cross-ply NCF laminates. A satisfactory agreement between the numerical and experimental failure stress, failure strain as well as the compressive stress-strain curves has been obtained for the MPDG method when using Maximum Stress, Hashin's or Puck's failure criteria.

Keywords

Composites; Non-crimp fabric (NCF); Finite element model (FEM); Compressive behaviour; Progressive damage; Failure mechanism.

1. Introduction

The attractive cost-performance relationship of non-crimp fabric (NCF) composites led to a substantial increase in their use in the past decade, particularly in the aerospace and automotive industries. The adoption rate of NCF composites has been increasing because they combine the benefits of automated manufacturing, easy handling and lower cost than the conventional woven fabric composites, with the superior mechanical properties of the unidirectional pre-impregnated tapes composites (UDPT).

NCF composites present a complex mesoscopic 3D structure that includes, for example, fibre tows in different in-plane orientations and with different cross-sections, resin rich areas, stitching yarns and fibre crimp due to the nesting of the tows or to the presence of the stitching yarns [1-5]. To illustrate these heterogeneities in the NCF structure at the mesoscopic scale, a typical NCF composite cross-section is shown in Fig. 1.

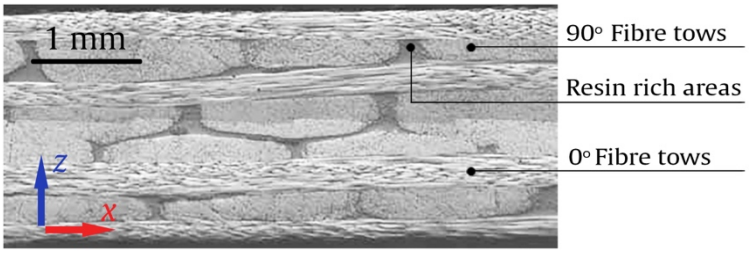

Fig. 1. Mesoscopic scale structure [1].

Numerical simulation, particularly finite element (FE) modelling, is often used to evaluate the mechanical performance of NCF composites prior to experimental characterisation. However, generating FE models that replicate the complex 3D structure of these materials requires establishing an important trade-off between accuracy and computational cost of the solution. Different approaches to model the mesoscopic 3D architecture of these materials can be found in literature. González et al. [6] developed a 3D meso-scale FE model of a $[0,90]_2$ NCF laminate with out-of-plane fibre crimped tows to study the apparent in-plane stiffness properties. Marklund and Asp [7] generated a 3D FE model with straight rectangular cross-section fibre tows in their study of combined micro-meso methodology for transverse matrix failure prediction and a similar approach was used by Mattsson et al. [8, 9] to study the performance of NCF laminate with different stacking sequences. Lomov et al. [10], in their study of meso-FE modelling of textile composites refer to the geometric modeller software, WiseTex, developed by Lomov and Verpoest [11], as a tool to create NCF composite geometries. This approach was used in [12-14] to generate the meso-scale structure of the NCF laminates and study their mechanical performance. Another geometric textile modeller software, Texgen, that resulted from the work of Robitaille et al. [15, 16] was also used by Serra Topal et al. [17] to generate a 3D non-crimp woven composite to study the last-stage fatigue damage. Even though these studies use different approaches to generate 3D FE models to evaluate the mechanical response of NCF composites under different types of loads, creating these 3D FE models efficiently is still a challenge.

A progressive damage model requires a stress analysis to obtain the stress distribution across the model, a failure criterion to estimate the initiation of damage, and a damage evolution law

to control the stiffness reduction of the damaged material. Currently, many damage models for composite materials can be found in literature. However, predicting their failure load still remains a challenge [18, 19]. Since the concept of damage was firstly presented by Kachanov [20] to study the creep rupture of metals, several other continuum damage mechanics approaches have been proposed to model damage progression [21-23]. Matzenmiller et al. [24] proposed the first damage model for fibre-reinforced composites in which the onset of damage was defined by Hashin's failure criterion [25] and the damage evolution was controlled by damage coefficients that reduce the stiffness of the material. Since then, other authors have also contributed to extend the number of approaches available to study damage progression in composite materials [26-29]. Various examples can be found in literature regarding the FE implementation of progressive damage models to composites [30-35].

In this study ANSYS® 18 [36] is employed to perform the numerical analyses, which allow us to choose between two distinct damage evolution methods: the material property degradation (MPDG) and the continuum damage mechanics (CDM). The MPDG method assumes that stiffness immediately reduces once the onset of material is reached and that the reduction is based on explicit values defined by damage coefficients which can take values from 0 (undamaged status) to 1 (completely damaged status). This method is a generalization of the concept of continuum damage evolution for composite laminates that was proposed by Camanho et al. [26]. In the CDM method, the damage coefficients increase progressively based on the energy amounts dissipated for the different damage modes (fibre tension, fibre compression, matrix tension and matrix compression). However, to be able to implement the CDM method, the material viscous damping coefficients and the energy dissipated per unit area need to be defined. Since these material properties were not available for the studied material, the MPDG method has been used in the progression damage model of the $[0,90]_n$ NCF laminate.

This paper is strongly related to previously published work [6, 37-39]. It follows the modelling approach presented in [37], which makes use of the rotation of the elements' coordinate system to model the fibre crimp in the geometrically straight 3D FE meshes. The efficiency/effectiveness of this approach was demonstrated in [6]. The qualitative mechanism responsible for the failure of NCF laminates under compressive loading was presented in [38], followed by a preliminary study to assess the quantitative value of the failure load using the Maximum Strain criterion and the MPDG method [39]. The current paper describes in greater detail the work initiated in [39] and extends the analysis by comparing different non-interactive (Maximum Stress and Maximum Strain) and interactive failure criteria (Hashin [25] and Puck [40]).

The description of the material properties, mesoscopic approach and the boundary conditions employed are presented in sections 2.1, 2.2 and 2.3, respectively. The progressive damage model used in the study is detailed in section 2.4. The progressive damage throughout the representative unit cell (RUC), from the load at which damage is initiated until the load at which the failure of the NCF laminate is predicted, is presented in section 3.1. The mechanisms responsible for the failure of the laminate are discussed in section 3.2. In section 3.3, the numerical results are validated against experimental results obtained from direct compression tests on biaxial cross-ply NCF laminates with similar average stiffness properties to those used in the numerical models [41]. Finally, the conclusions are presented in section 4.

2. Numerical Modelling

The following subsections are dedicated to describing the material properties of the constituents, the mesoscopic modelling approach, the boundary conditions and the progressive damage model used in the generation of the FE model.

2.1. Material properties of the constituents

Fibre tows can be considered, at the mesoscopic scale, as a homogeneous transversely isotropic material made from parallel fibres uniformly distributed and impregnated by an isotropic resin. Since no experimental measurements have been performed to evaluate the elastic constants of the fibre tows, the corresponding stiffness matrix in the FE model has been calculated using micro-meso homogenisation, based on Chamis' semi-empirical model [42]. This micromechanical model has been used in several studies of meso-FE modelling for textile composites as it gives the formulation for all independent elastic constants [43-45]:

$$E_{11} = V^f E_{11}^f + \left(1 - V^f\right) E^m \quad ; \quad E_{22} = E_{33} = \frac{E^m}{1 - \sqrt{V^f}} \left(1 - \frac{E^m}{E_{22}^f}\right) \tag{1}$$

$$G_{12} = G_{13} = \frac{G^m}{1 - \sqrt{V^f} \left(1 - \frac{G^m}{G_{12}^f}\right)} \quad ; \quad G_{23} = \frac{G^m}{1 - \sqrt{V^f} \left(1 - \frac{G^m}{G_{23}^f}\right)} \tag{2}$$

$$\nu_{12} = \nu_{13} = V^f \nu_{12}^f + \left(1 - V^f\right) \nu^m \quad ; \quad \nu_{23} = \frac{E_{22}}{2G_{23}} - 1 \tag{3}$$

where V^f is the fibre volume fraction of the tows and E, G and ν are elastic moduli, shear moduli and Poisson's ratios, respectively. Superscript f is used for the fibre properties while superscript m is used for the matrix properties. Subscript 1 designates the longitudinal fibre direction while 2 and 3 designate the transverse fibre directions in the material (3 being the through-thickness direction of the laminate).

The constituents of the biaxial cross-ply NCF composites, tested under direct compression for the FALCOM project and presented in Table 1, have been considered in the estimation of the elastic properties of the fibre tows [41]. The epoxy resin - Hexply® M36 [46] is characterized by, $E^m = 3.5$ GPa, $\nu^m = 0.42$ and $G^m = 1.2$ GPa. The carbon fibre Tenax® HTS 5631 12K [47] is characterized by, $E_{11}^f = 237$ GPa, $E_{22}^f = 13$ GPa, $\nu_{12}^f = 0.2$, $G_{12}^f = 18$ GPa, $G_{23}^f = 6$ GPa. Notice that the elastic properties of the carbon fibres have been extracted from the manufacturer's datasheet and those which were not available have been obtained from literature, using averaged values derived from experimental measurements [42, 47-52].

Parameter	Description/Value
Representative unit cell size	[x] 2.6 mm × [y] 2.6 mm × [z] 0.96 mm
Tows	Carbon fibre - Tenax® HTS 5631 12K
Matrix	Epoxy resin - Hexply® M36

Table 1. $[0,90]_n$ NCF laminate parameters.

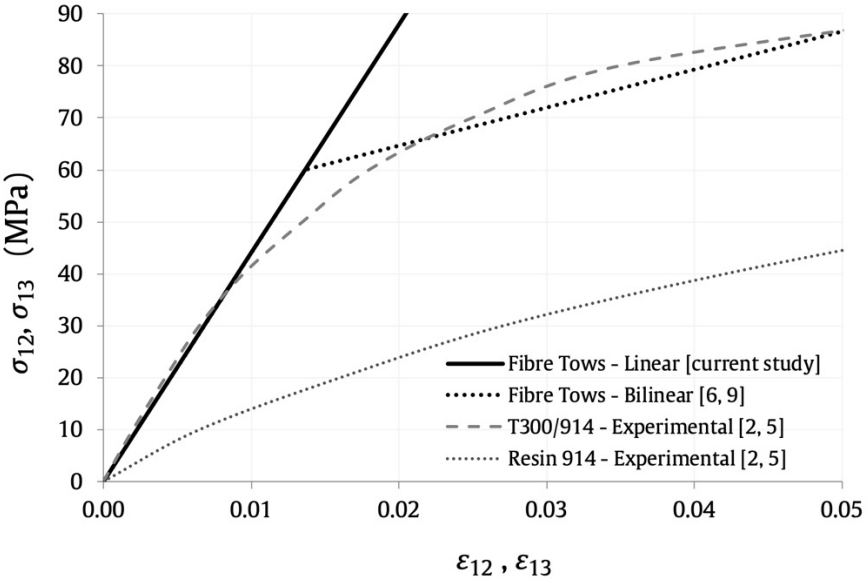

Fig. 2. Shear stress-strain behaviour of the fibre tows.

The behaviour of the fibre tows under shear loads in the 12-plane and 13-plane, is controlled by the resin, whose behaviour is nonlinear [2, 5, 53]. This nonlinear behaviour can be appreciated in Fig. 2, in which the shear stress-strain experimental curve obtained from a unidirectional laminate T300/914 is represented [2, 5, 53]. In previous studies [37, 38], the bilinear behaviour was included in the RUC to account for the shear nonlinear behaviour of the fibre tows. Notwithstanding, to be able to carry out a progressive damage study with ANSYS® 18 [36], the fibre tows have been modelled with a linear elastic shear behaviour in all planes, as both material behaviour models cannot be added simultaneously to the FE model.

The fibre tows have been defined with an averaged fibre volume fraction of 60% taking into consideration the values observed in [54]. The estimated stiffness properties of the fibre tows are presented in Table 2.

E_{11}	$E_{22} = E_{33}$	$\nu_{12} = \nu_{13}$	ν_{23}	$G_{12} = G_{13}$	G_{23}
147 GPa	8.1 GPa	0.29	0.26	4.43 GPa	3.2 GPa

Table 2. Estimated stiffness properties of the fibre tows.

The strength properties of the fibre tows have been obtained from averaged strength values of carbon fibre unidirectional laminates with a fibre volume fraction of 60% [55, 56]. The values employed are presented in Table 3, where S_{ij}^{l} are the strengths of the fibre tows with indices $i, j = 1, 2, 3$ corresponding to the aforementioned orthogonal directions, and $l = +, -, s$ standing for the fibre tows tensile, compressive and shear strength, respectively.

The strain limits used in the Maximum Strain criterion have been calculated dividing the strength limits by the appropriate stiffness coefficients, i.e., assuming a linear relationship [55, 57].

S_{11}^{+}	S_{11}^{-}	$S_{22}^{+} = S_{33}^{+}$	$S_{22}^{-} = S_{33}^{-}$	$S_{12}^{s} = S_{13}^{s} = S_{23}^{s}$
2100 MPa	1500 MPa	55 MPa	200 MPa	67 MPa

Table 3. Strength properties of the fibre tows.

2.2. Mesoscopic approach of the NCF laminate

A mesoscopic scale FE model of the RUC of a $[0,90]_n$ NCF laminate has been modelled using 3D 8 node (three degrees of freedom at each node) solid element SOLID185 from ANSYS® 18 FE code [36]. This element enables the definition of an element's coordinate system with an orientation not imposed by the node locations, thus allowing us to define the orthotropic material directions appropriately at each point.

Each lamina of the unit cell is composed of two halves of a fibre tow which are separated by a resin rich area. The stacking sequence and the fibre tows orientation and shape are represented in Fig. 3. Although the fibre tows have been generated using a straight 3D FE mesh, an out-of-plane fibre crimp has been modelled following the approach presented in [37]. The fibre crimp has been defined with the same maximum angle ($\beta = 9°$) and transversal to the fibre direction in all fibre tows. The fibre crimp orientation, upwards or downwards, has been made dependent on the lamina stack position in the laminate. To ensure the appropriate modelling of the fibre crimp and to improve the accuracy of the numerical solution, the FE mesh has been refined inside and around the fibre crimp locations. Notice that the maximum fibre crimp angle that has been employed in the FE model was defined based on previous studies [6, 58], in which (using an identical RUC) a satisfactory agreement has been found between the apparent in-plane stiffness properties and the experimental evidence for angles ranging from 9º to 12º.

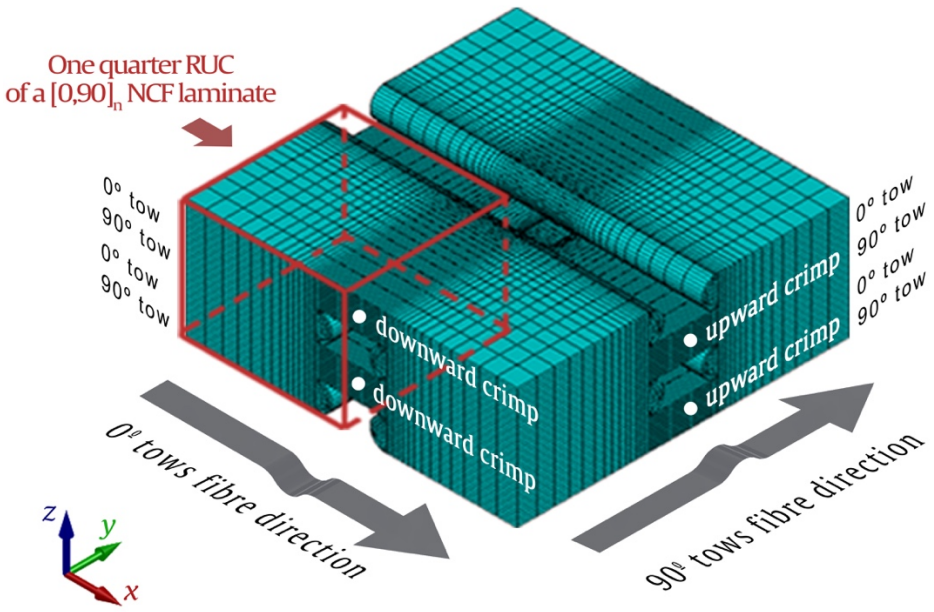

Fig. 3. 3D FE model of the RUC of the $[0,90]_n$ NCF laminate (fibre tows only).

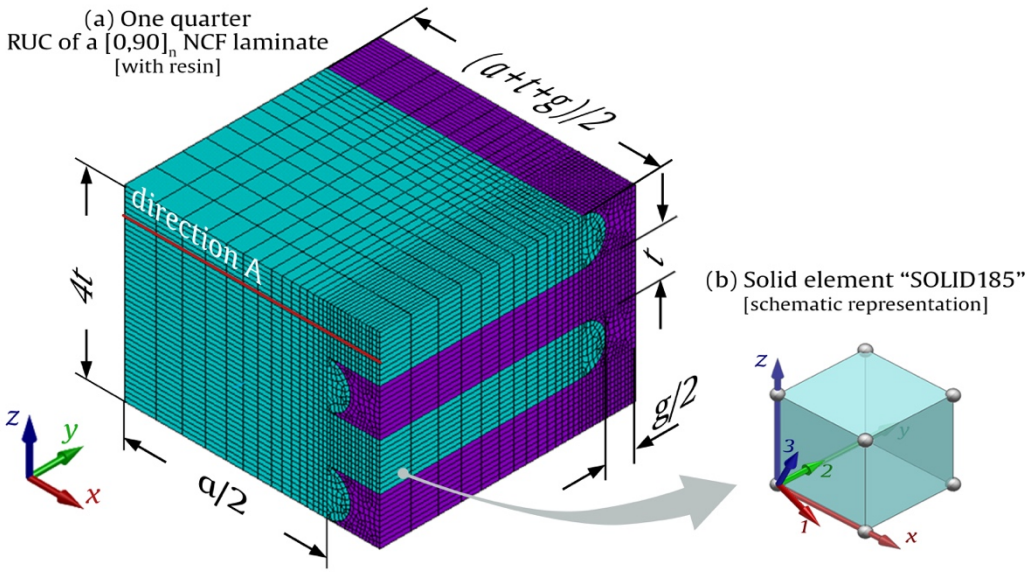

Fig. 4. (a) One-quarter of the 3D FE model of the RUC of the $[0,90]_n$ NCF laminate with geometric parameters. (b) rotation of the element's coordinate system.

Taking advantage of the symmetry of the problem, only one-quarter of the RUC has been modelled in this study, see Fig. 4(a). The RUC has been defined parametrically with the geometric parameters being the length of the tow not affected by the fibre crimp (a=2.06 mm), the thickness of each lamina (t=0.24 mm), and the width of the gap left between two adjacent tows of each lamina (g=0.3 mm), see Fig. 4(a). The values used in the dimensioning of the RUC (a, t and g) were estimated from the microstructure characterization performed in [48] and the total size of the RUC is shown in Table 1.

In accordance with the global coordinate system *xyz*, the plane of the laminate is the *xy*-plane, and *z* is the through-thickness direction while the local coordinate system *123* is oriented considering the actual direction of the fibres, direction *1* in Fig. 4(b).

As an indication, the quarter of the RUC of the $[0,90]_n$ NCF laminate shown in Fig. 4a) has a total of 36952 elements and 150121 nodes.

2.3. Boundary conditions

The boundary conditions applied to the faces of the FE model serve to impose a compressive stress state and to guarantee the displacements compatibility in the limits of the model with the surrounding structure. Symmetry conditions have been assumed at the faces parallel to the *xz*-plane and at one of the faces parallel to *yz*-plane, while at the opposite face, parallel to the *yz*-plane, a constant displacement in the compression load direction has been applied to all nodes. In this way, the compression load is given by the sum of the reaction forces of all nodes at $x = 0$. The boundary conditions at the top and bottom faces (parallel to the *xy*-plane) must guarantee the compatibility of the unit cell under consideration with the adjacent unit cells. Thus, the displacements of the nodes at both faces were coupled to assure that the extension in the through-thickness direction is constant throughout the entire model.

2.4. Progressive damage modelling

Progressive damage has been modelled at the mesoscopic level using the built-in MPDG method, available in ANSYS®18 [36]. This damage evolution method requires the definition of a damage initiation criteria to determine the onset of the material damage, and a damage evolution law that controls the stiffness reduction of the material.

Since there are no well-established specific damage initiation criteria for NCF composites, and given that at this scale fibre tows can be considered to behave as UD composite laminas, the most commonly used failure criteria for laminates [57] have been applied to the fibre tows to predict the onset of the material damage and its progression until the compressive failure of the NCF laminate. Non-interactive criteria, Maximum Stress and Maximum Strain, and interactive criteria, Hashin [25] and Puck [40], have been employed to determine the onset of the material damage of the fibre tows under the compressive loading (see Appendix A).

For the sake of simplification and knowing beforehand that the material degradation of the resin rich areas will have a very small impact on the overall stiffness reduction of the NCF laminate, the Maximum Stress criterion has been employed for all the resin rich areas. Notice that all the required tensile and compressive strengths for the resin are available in the manufacturer's datasheet [46].

According to the MPDG method, after reaching the onset of the material damage defined by each criterion, the stiffness reduction occurs immediately, and each damage mode (fibre tension, fibre compression, matrix tension and matrix compression) is assumed to be uncoupled. The amount of stiffness reduction is based on damage coefficients specified in the damage evolution law. These coefficients can vary from 0 to 1, where 0 corresponds to no damage and 1 to the complete loss of stiffness in the affected damage mode.

The Hooke's law for a damaged orthotropic material is given by (4), where $\boldsymbol{S_{ij}}$ are the components of the compliance matrix of the undamaged orthotropic material, $\boldsymbol{\sigma}$ is the nominal Cauchy stress tensor, and $\boldsymbol{\varepsilon}$ is the elastic strain tensor [11].

$$\boldsymbol{\varepsilon} = \begin{bmatrix} \frac{S_{11}}{(1-d_f)} & S_{12} & S_{13} & 0 & 0 & 0 \\ S_{21} & \frac{S_{22}}{(1-d_m)} & S_{23} & 0 & 0 & 0 \\ S_{31} & S_{32} & \frac{S_{33}}{(1-d_m)} & 0 & 0 & 0 \\ 0 & 0 & 0 & \frac{S_{44}}{(1-d_s)} & 0 & 0 \\ 0 & 0 & 0 & 0 & \frac{S_{55}}{(1-d_s)} & 0 \\ 0 & 0 & 0 & 0 & 0 & \frac{S_{66}}{(1-d_s)} \end{bmatrix} \boldsymbol{\sigma} \qquad (4)$$

The damage coefficients for calculating the damaged elasticity matrix are determined by,

$$d_f = \begin{cases} d_f^+, if\ I_f^+ \geq 1 \\ d_f^-, if\ I_f^- \geq 1 \end{cases}$$

$$d_m = \begin{cases} d_m^+, if\ I_m^+ \geq 1 \\ d_m^-, if\ I_m^- \geq 1 \end{cases} \quad (5)$$

$$d_s = 1 - \left(1 - d_f^+\right)\left(1 - d_f^-\right)\left(1 - d_m^+\right)(1 - d_m^-)$$

where, d_s is the shear damage coefficient and I_f^+, I_f^-, I_m^+ and I_m^- are respectively the fibre tension, fibre compression, matrix tension and matrix compression damage initiation indexes calculated from the effective Cauchy stress measured in the undamaged domain. Each criterion computes the damage initiation indexes differently [25, 40], hence different progressive damage results are obtained with the Hashin's, Puck's, Maximum Stress and Maximum Strain failure criteria.

As mentioned before, there are no well-stablished failure criteria for a fibre tow of an NCF laminate, so several criteria that were initially developed for a prepreg lamina were object of analysis in this study: Maximum Stress, Maximum Strain, Puck and Hashin. Therefore, four different progressive damage FE models have been generated. In all of them, the matrix has been modelled as an isotropic material and the onset of failure has been estimated with the Maximum Stress criterion. Otherwise, the fibre tows have been modelled as a transversely isotropic material and a different failure criterion to estimate the onset of damage has been used in each of the four models. Notice also that each of these failure criteria is in fact a close set of four different failure criteria associated to the four different damage modes (fibre tension, fibre compression, matrix tension and matrix compression).

The damage coefficients values employed in this study for the fibre tows and for the resin rich areas (fibre tension, d_f^+, fibre compression, d_f^-, matrix tension, d_m^+, and matrix compression, d_m^-) are presented in Table 4. A parametric study has been carried out to select the damage coefficients which produce results that better adjust to the experimental evidence.

In the parametric study, different damage coefficient values, ranging from 0 to 0.4, have been considered for both the fibre tows and for the resin rich areas. The results have shown that for the resin rich areas, changing the matrix damage coefficient values, d_m^+ and d_m^-, within this range, adds no relevant effect on the stiffness degradation of the NCF laminate.

However, for the fibre tows, the sensitivity to changes in the coefficients values has shown to be much higher. The matrix damage coefficients, d_m^+ and d_m^-, control the amount of the initial stiffness reduction of the *damaged* elements. At this stage, the fibre damage coefficients are still not initiated $\left(d_f^+ = d_f^- = 0\right)$. The amount of the second and last stiffness reductions in the *completely damaged* elements are controlled by all the damage coefficient values, d_m^+, d_m^-, d_f^+ *and* d_f^-. In this way, it is clear that the damage coefficients used in the fibre tows can control both the nonlinear behaviour and the failure load of the NCF laminate. The relation between the damage coefficient values and the stiffness reductions is addressed with greater detail in the next section.

Notice that setting any of the damage coefficients values above 0.4, either for the fibre tows or the resin rich areas, caused large stiffness reductions in the affected elements just after the onset of the material damage had been reached. As a consequence, the affected elements experienced large distortions and the solutions failed to converge.

	Fibre Tension $[d_f^+]$	Fibre Compression $[d_f^-]$	Matrix Tension $[d_m^+]$	Matrix Compression $[d_m^-]$
Fibre tows	0.3	0.3	0.25	0.25
Resin rich areas	-	-	0.25	0.25

Table 4. Damage coefficient values used in the numerical model.

3. Numerical results

In this section, the results of the damage initiation and its progression throughout the RUC, are presented.

The numerical solutions have been obtained with ANSYS®18 [36], 64-bit version, with standard memory and CPU management, the computation time required for each solution has been approximately 50 minutes on a PC with Intel Core i7 and 8GB RAM.

3.1. Damage progression until failure of the NCF laminate

The progressive damage throughout the unit cell from the load at which damage is initiated, until the load at which the failure of the laminate is predicted is presented in this section.

	Hashin [MPDG]	Max. Stress [MPDG]	Max. Strain [MPDG]	Puck [MPDG]	Experimental [41]	
					Average	St. Dev.
Damage initiation (Stress)	210 MPa	250 MPa	270 MPa	250 MPa	-	-
Damage initiation (Strain)	0.31%	0.38%	0.41%	0.38%	-	-
Failure stress	648 MPa	645 MPa	575 MPa	650 MPa	676 MPa	46 MPa
Failure strain	1.07%	1.07%	0.94%	1.06%	1.08%	0.09%

Table 5. Numerical and experimental values of damage initiation and failure stress and strain.

The numerical results show that damage initiation depends on the failure criterion considered in the FE model. In this study, damage was predicted to initiate for strain values, ε_{11}, between 0.31% and 0.41%, see Table 5. However, independently of the criterion, the first *damaged* elements arise within the 0° fibre tows, particularly in the crimped elements with higher misorientation angle, see Fig. 5a) and Fig. 5b). As is detailed in section 3.2, this is caused by the high localized shear stresses, σ_{13}, and shear strains, ε_{13}, that develop in this location, and that exceed the allowable shear strength, S_{13}^s, that has been defined in the numerical model for the fibre tows. Therefore, the shear damage coefficient ($d_s = 0.437$) is activated and its value is calculated from the matrix damage coefficients values defined for the fibre

tows $\left(d_m^+ = d_m^- = 0.25\right)$, see Eq. (5). Since any of the other allowables of the fibre tows has been exceeded, the fibre damage coefficients are not initiated at this stage $\left(d_f^+ = d_f^- = 0\right)$.

The number of *damaged* elements progressively increases within the crimp location after the onset of material damage, causing a nonlinear response in the NCF laminate, see Fig. 5b) and Fig. 6.

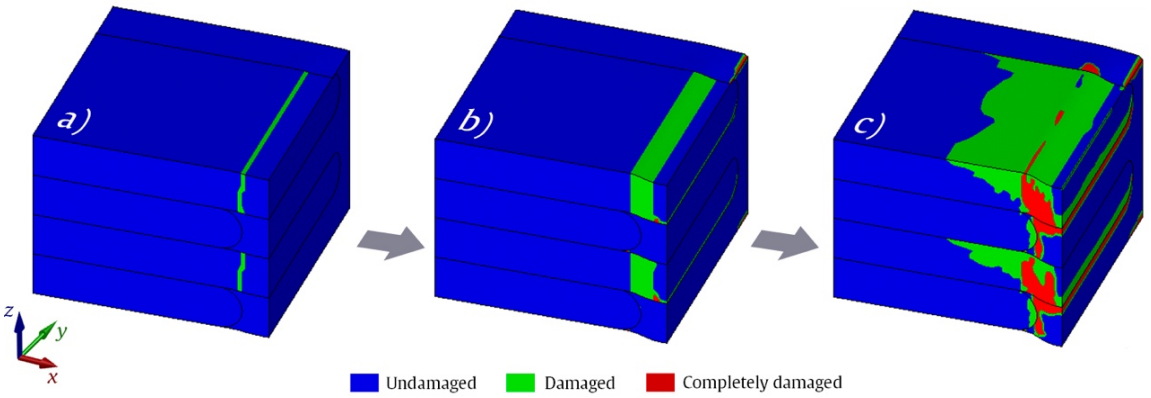

Fig. 5. Damage evolution throughout the RUC.
a) Damage initiation, b) Damage propagation, c) Predicted failure of the laminate.

The first *completely damaged* elements appear in the fibre crimp location of the 0° tows independently of the failure criteria. At this stage, all the damage coefficients are initiated in these elements $\left(d_m^+ = d_m^- = 0.25, d_f^+ = d_f^- = 0.3 \text{ and } d_s = 0.724\right)$, which results in the second and last instant degradation of their stiffness properties. For the Hashin's, Puck's and the Maximum Stress failure criteria, the *completely damaged* elements arise for approximately the same compressive load ($\sigma_{11} \cong 580$ MPa), while for the Maximum Strain criterion they arise for a lower compressive load, ($\sigma_{11} \cong 520$ MPa), see Fig. 6. These loads for which the first *completely damaged* elements appear, correspond approximately to 90% of the failure load predicted by each failure criterion.

Subsequently, the *damaged* and *completely damaged* elements spread rapidly, mainly throughout the 0° fibre tows and the resin rich areas below the fibre crimp location, see Fig. 5c). This sequence of events motivates the sudden loss of the NCF laminate stiffness, the failure of the NCF laminate being then predicted.

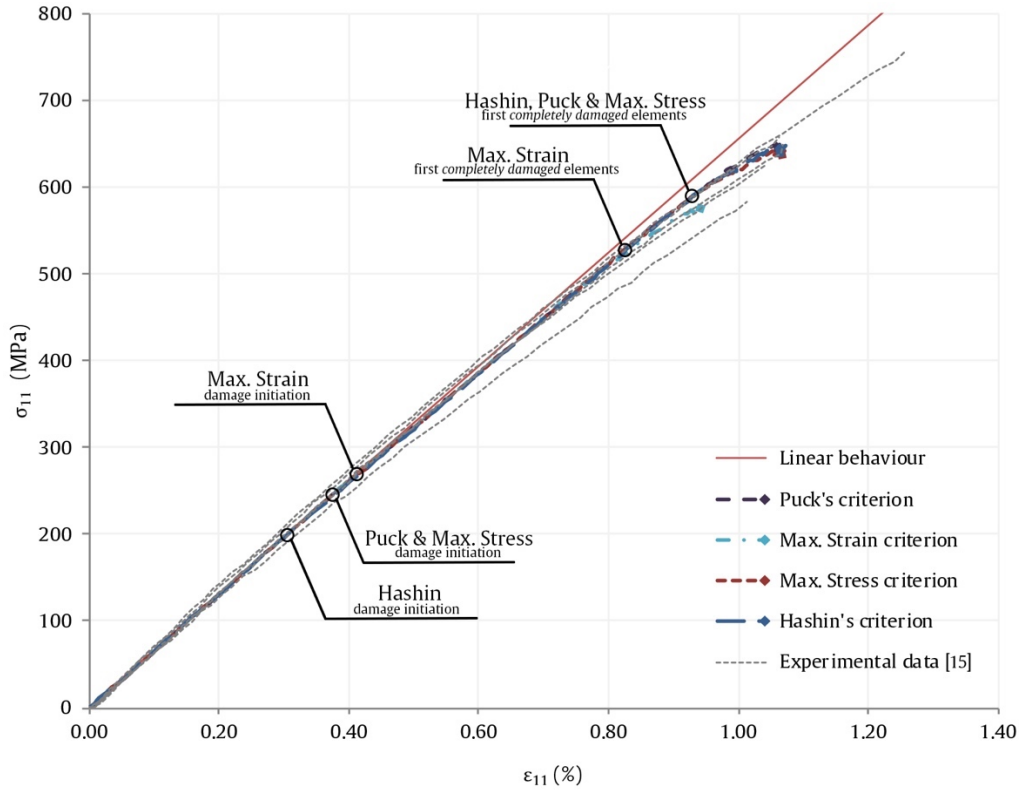

Fig. 6. Numerical and experimental stress-strain curves.

Notice in Fig. 6 that all the numerical stress-strain curves show a similar behaviour and a satisfactory agreement with the experimental evidence [41]. Despite of the differences in the load in which onset of damage is predicted, which cannot be correlated with the experiments, all models show a low stiffness reduction, similar to that shown in the experimental curves, until the ultimate load is reached. As mentioned before, the ultimate loads obtained with the models are very similar and in very good agreement with the average of the experimental results. As mentioned in section 2.4, a preliminary parametric study was performed to determine the values that best fitted the experimental evidence, among those that allow the solution to converge.

3.2. Mechanisms responsible for failure

In previous studies [37, 38, 59], it was demonstrated that the out-of-plane fibre crimp along with the compressive load are responsible for an instability phenomenon that causes the development of high localized shear stresses, σ_{13}, and shear strains, ε_{13}, in the 0° fibre tows. These studies are in agreement with the results presented in section 3.1, in which damage is predicted to initiate in the fibre crimp location, it being also responsible for the predicted failure of the NCF laminate. The aforementioned high shear stress-strain gradients in the fibre crimp location can be appreciated in Fig. 7, where the shear stresses, σ_{13}, and shear strain, ε_{13}, are plotted at $\varepsilon_{11} = 0.4\%$ (just after the onset of the material damage in the Maximum Stress criterion model).

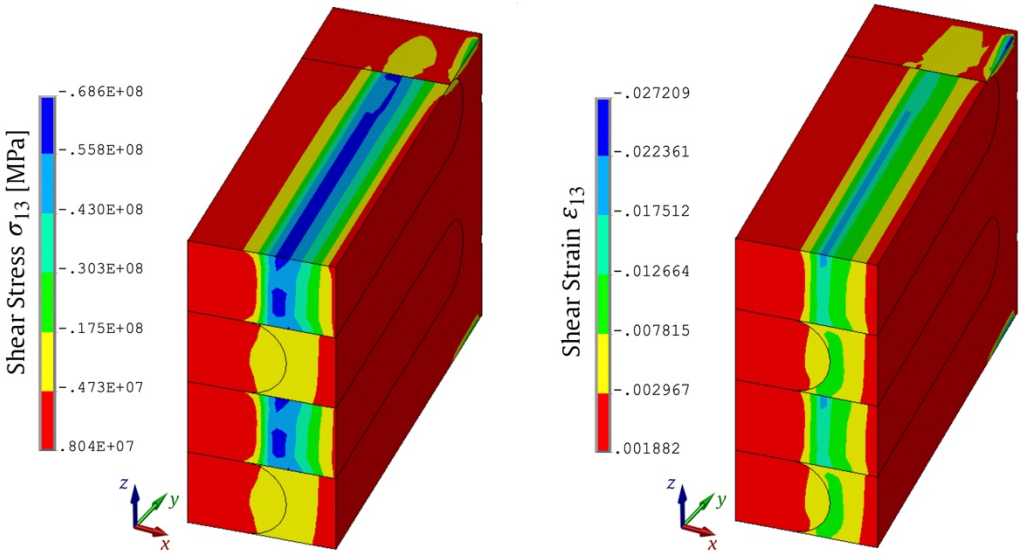

Fig. 7. Shear stress and shear strain after damage initiation, $\varepsilon_{11} = 0.4\%$, (Maximum Stress criterion).

The values of the Maximum Stress criterion components, $\left|\sigma_{11}/S_{11}^{-}\right|$, $\left|\sigma_{13}/S_{13}^{s}\right|$, $\left|\sigma_{22}/S_{22}^{-}\right|$ and $\left|\sigma_{33}/S_{33}^{-}\right|$, along a line in the middle of a 0° tow (*direction A* shown in Fig. 4) for the same instance, $\varepsilon_{11} = 0.4\%$, are represented in Fig. 8. The misorientation angle of the elements along the same direction has also been included to help in the understanding of the relationship between the failure initiation and the fibre crimp angle.

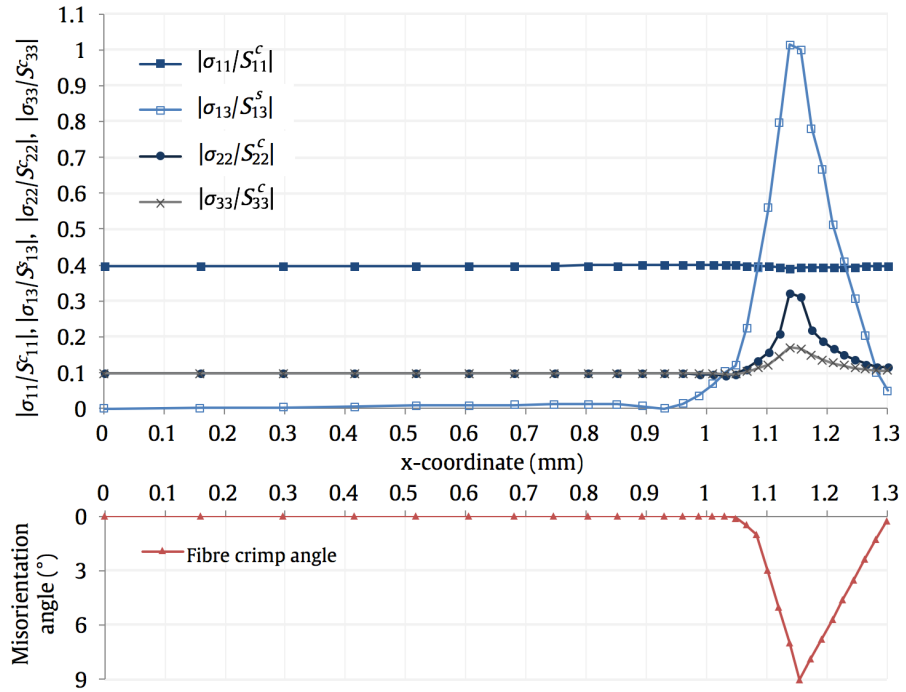

Fig. 8. Maximum Stress criterion components and misorientation angle along *direction A* at $\varepsilon_{11} = 0.4\%$.

Knowing that the Maximum Stress criterion states that failure initiates when a stress component exceeds the respective allowable and that there is no interaction between the different stress components, it is shown in Fig. 8 that only shear stresses σ_{13} are contributing to the failure initiation, $\left|\sigma_{13}/S_{13}^{s}\right| \geq 1$. Moreover, it is also shown that damage initiates in the elements with maximum misorientation angle, that is when the fibre crimp angle reaches 9°. According to the progressive damage model, this motivates the instant degradation of the shear behaviour of those elements as well as the nonlinear response of the NCF laminate.

The averaged damage evolution of an element with the maximum misorientation angle in a 0° fibre tow, using the Maximum Stress as the damage initiation criterion, is represented in Fig. 9. Notice that each small circle corresponds to the result of a load step of the non-linear analysis.

The element remains *undamaged* until it reaches the onset of the material damage defined by the failure criterion, which is represented by load step *(a)*. Before the element becomes *damaged*, it presents an intermediate shear stiffness reduction, shown as load step *(b).* At this load step, not all nodes of the element have reached the *damaged* status, hence the averaged nodal results of the considered 3D solid element present a lower stiffness reduction. At load step *(c)*, the element status is finally defined as *damaged* and according to the values assigned to the damage coefficients in the MPDG method, and considering (5), the shear stiffness of the element decreases by 43.7%. This shear stiffness is kept unchanged until load step *(e).* As soon as all the damage coefficients are activated, the element becomes *completely damaged* and the initial shear stiffness of the element decreases by 72.4% (based on the values assigned to the damage coefficients). This latter status is initiated in load step *(g)*. As for the intermediate shear stiffness reduction that occurred between the *undamaged* and *damaged* element status, there are also some intermediate load steps between the *damaged* and the *completely damaged* element status, as the one represented by *(f)*. An elastic recovery of the element can be appreciated between load steps *(d)*, *(e)* and after step *(g)*. This behaviour may be related to the fact that the analysis has been defined assuming large displacements or to the stress relaxation associated with the change of stiffness in the surrounding elements. Finally, after reaching the maximum load step *(h)*, the laminate is predicted to fail, which is a consequence of the substantial increase in the number of *completely damaged* elements in the laminate.

Analogous behaviour can be appreciated for all the failure criteria considered in this study, see Fig. 10.

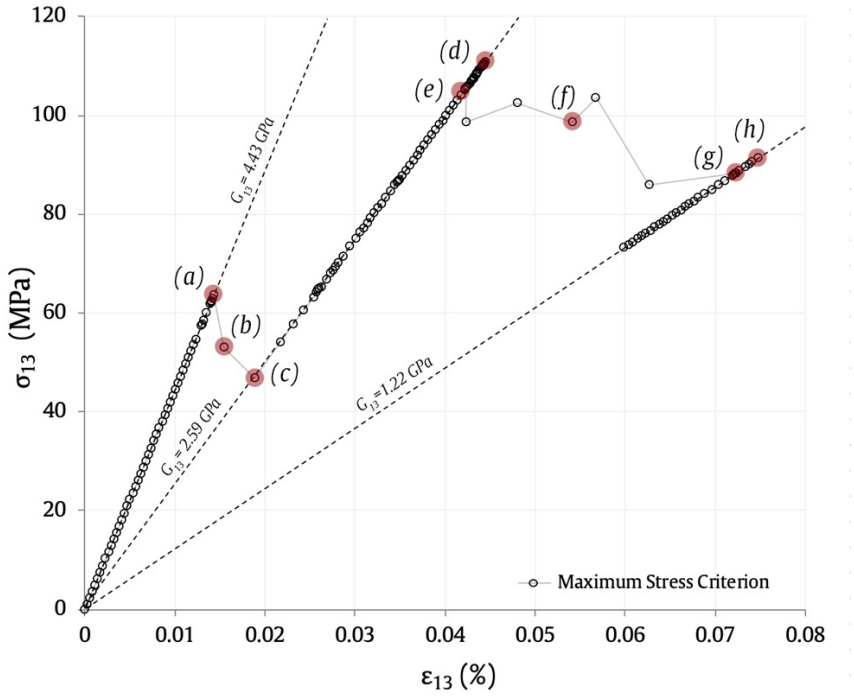

Fig. 9. Damage development analysis for an element with maximum misorientation in a 0° fibre tow for the Maximum Stress criterion.

The different damage initiation loads for the failure criteria, can also be appreciated in shear stress-strain results presented in Fig. 10. Moreover, it is possible to observe, that independently of the failure criterion, all elements have the same stiffness once they reach the *damaged* and *completely damaged* status. This is due to the fact that the same damage coefficients have been used in the different failure criteria.

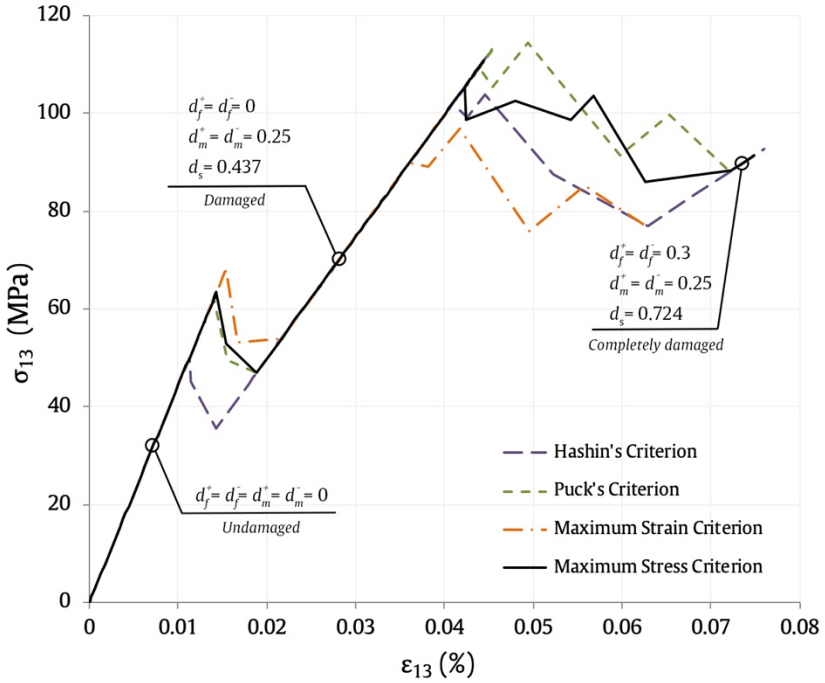

Fig. 10. Damage development analysis for an element with maximum misorientation in a 0° fibre tow for all the failure criteria.

As can be seen, results shown in Fig. 10 are in a fairly good agreement with the non-linear shear behaviour of the fibre tows shown in Fig. 2. Notice that, material degradation is used to model the non-linear shear behaviour of the fibre tows since, as already mentioned, ANSYS® 18 [36] does not allow us to use two non-linear material models at the same time. However, the existence of different failure indexes and damage coefficients associated to different failure modes has made possible to obtain good agreement with experimental results using the progressive damage to model both the failure and the non-linear shear response of the material.

3.3. Failure load predictions comparison and validation of the numerical results.

The numerical predictions of failure stress and failure strain, for each failure criteria, are discussed in this section. The numerical results are also validated against the experimental data obtained from direct compression tests on biaxial cross-ply NCF laminates with similar average stiffness properties to those used in the numerical models [41].

The results presented in Table 5 and Fig. 6, make evident the similarity in the failure stress and failure strain values obtained for the Hashin's, Puck's and the Maximum Stress failure criteria. The predicted failure stress and failure strain are almost identical for all the aforementioned criteria, with values between 645-650 MPa and 1.06-1.07%, respectively. The experimental mean values for the failure stress and failure strain are only 4% and 1% higher than the numerically predicted results, respectively. The Maximum Strain criterion predicted approximately a failure stress and failure strain values 10-14% lower than the all other criteria. This difference is justified by the fact that the strain limits have been calculated dividing the strength limits by the initial stiffness coefficients.

The compressive elastic modulus is another relevant parameter for the validation of the numerical models. The stiffness of the $[0,90]_n$ NCF laminate has been calculated for a strain of $\varepsilon_{11} \cong 0.01\%$ (no damage initiation). The numerical and the experimental mean values of the compressive elastic modulus are in satisfactory agreement as is possible to appreciate from the stress-strain curves represented in Fig. 6. The numerical and experimental mean values obtained are, $E_x^{num} = 65.5$ GPa and $E_x^{exp} = 67.4$ GPa, respectively.

4. Conclusions

A mesoscopic 3D RUC has been used to study the progressive damage of a $[0,90]_n$ NCF laminate under in-plane compressive loading. The RUC has been defined with an out-of-plane fibre crimp with a maximum misorientation angle of $\beta = 9°$ in the 0° fibre tows. The material properties degradation method has been used in this study and non-interactive criteria (Maximum Stress and Maximum Strain), and interactive criteria (Hashin and Puck), associated with failure modes, have been employed to determine the onset of the material damage of the fibre tows. The Maximum Stress criterion has been used for all the resin rich areas.

The following stages have been identified in the analysis of the progressive damage of the NCF laminate when submitted to the compressive loading. Firstly, the presence of high localized shear stresses, σ_{13}, and shear strains, ε_{13}, in the crimp location of the 0° fibre tows,

particularly in elements with higher misorientation angle, are responsible for the damage initiation, i.e., they exceed the respective allowable that has been defined in the numerical model. Secondly, once the onset of the material damage is reached, the affected elements become *damaged* and suffer an instant stiffness reduction based on the values defined for the damage coefficients. Thirdly, damage propagates to the surrounding elements of the fibre crimp location and *completely damaged* (all damage coefficients are initiated) elements also arise, suffering then a second stiffness reduction. Finally, both *damaged* and *completely damaged* elements spread rapidly, mainly throughout the 0° tows and the resin reach areas below the crimp location. These events motivate the sudden loss of the NCF laminate stiffness, and thus failure of the NCF laminate is predicted, see Fig. 5.

The numerical results obtained with the MPDG method in which the onset of the material damage was determined by Hashin's, Puck's and Maximum Stress criteria presented a satisfactory agreement with the experimental data. On the other hand, the MPDG method combined with the Maximum Strain criterion predicted values outside the range of the experimented results.

A satisfactory agreement between the numerically calculated compressive elastic modulus of the $[0,90]_n$ NCF laminate and the experimental mean values has been found. The results have also shown that the shear modulus of the tows does not substantially affect the compressive elastic modulus of the NCF laminate.

The scope of the study can be widened in the future to include also the Continuum Damage Mechanism (CDM) method available in ANSYS® 18 [36] which uses the Hashin's failure criterion to predict the onset of the material damage.

Appendix A

The expressions employed to compute damage initiation indexes in ANSYS® 18 [36] for the non-interactive criteria (Maximum Stress and Maximum Strain) and the interactive criteria (Hashin and Puck), are summarized in Table 6 and Table 7, respectively.

	Maximum Stress Failure Criterion	**Maximum Strain Failure Criterion**
Fibre Tension: $\sigma_{11} > 0$	$I_f^+ = \frac{\sigma_{11}}{S_{11}^+}$	$I_f^+ = \frac{\varepsilon_{11} E_{11}}{S_{11}^+}$
Fibre Compression $\sigma_{11} < 0$	$I_f^- = \frac{\sigma_{11}}{S_{11}^-}$	$I_f^- = \frac{\varepsilon_{11} E_{11}}{S_{11}^-}$
Matrix Tension $\sigma_{22}, \sigma_{33} > 0$	$I_m^+ = \frac{\sigma_{22}}{S_{22}^+}, \quad I_m^+ = \frac{\sigma_{33}}{S_{33}^+}$	$I_m^+ = \frac{\varepsilon_{22} E_{22}}{S_{22}^+}, \quad I_m^+ = \frac{\varepsilon_{33} E_{33}}{S_{33}^+}$
Matrix Compression $\sigma_{22}, \sigma_{33} < 0$	$I_m^- = \frac{\sigma_{22}}{S_{22}^-}, \quad I_m^- = \frac{\sigma_{33}}{S_{33}^-}$	$I_m^- = \frac{\varepsilon_{22} E_{22}}{S_{22}^-}, \quad I_m^- = \frac{\varepsilon_{33} E_{33}}{S_{33}^-}$

Table 6. Non-interactive failure criteria associated with failure modes.

Hashin's Failure Criterion [25, 36]	
Fibre Tension $\sigma_{11} \geq 0$	$I_f^+ = \left(\frac{\sigma_{11}}{S_{11}^+}\right)^2 + \frac{\sigma_{12}^2 + \sigma_{13}^2}{\left(S_{12}^s\right)^2}$
Fibre Compression $\sigma_{11} < 0$	$I_f^- = \left(\frac{\sigma_{11}}{S_{11}^-}\right)^2$
Matrix Tension $\sigma_{22} + \sigma_{33} > 0$	$I_m^+ = \frac{(\sigma_{22} + \sigma_{33})^2}{\left(S_{11}^+\right)^2} + \frac{\sigma_{23}^2 - \sigma_{22}\sigma_{33}}{\left(S_{23}^s\right)^2} + \frac{\sigma_{12}^2 + \sigma_{13}^2}{\left(S_{12}^s\right)^2}$
Matrix Compression $\sigma_{22} + \sigma_{33} < 0$	$I_m^- = \frac{1}{S_{22}^-}\left[\left(\frac{S_{22}^-}{2S_{23}^s}\right)^2 - 1\right](\sigma_{22} + \sigma_{33}) + \left(\frac{\sigma_{22} + \sigma_{33}}{2S_{23}^s}\right)^2 + \frac{\sigma_{23}^2 - \sigma_{22}\sigma_{33}}{\left(S_{23}^s\right)^2} + \frac{\sigma_{12}^2 + \sigma_{13}^2}{\left(S_{12}^s\right)^2}$
Puck's Failure Criterion [36, 60]	
Fibre Tension $\sigma_{11} \geq 0$	$I_f^+ = \frac{\sigma_{11}}{S_{11}^+}$
Fibre Compression $\sigma_{11} < 0$	$I_f^- = \frac{\sigma_{11}}{S_{11}^-}$
Inter-fibre Tension [Matrix Tension] $\sigma_n \geq 0$	$I_m^+ = \sqrt{\left(\frac{1}{S_{22}^+} - K^+\right)^2 \sigma_n^2 + \left(\frac{\tau_{nt}}{S_{23}^s}\right)^2 + \left(\frac{\tau_{n1}}{S_{12}^s}\right)^2} + K^+\sigma_n$ $K^+ = \begin{cases} \frac{1}{\tau_{nt}^2 + \tau_{n1}^2}\left(\frac{P_{23}^+}{S_{23}^s}\tau_{nt}^2 + \frac{P_{13}^+}{S_{12}^s}\tau_{n1}^2\right) & \text{if } \tau_{nt}^2 + \tau_{n1}^2 > 0 \\ 0 & \text{if } \tau_{nt}^2 + \tau_{n1}^2 = 0 \end{cases}$
Inter-fibre Compression [Matrix Compression] $\sigma_n < 0$	$I_m^- = \sqrt{\left(\frac{\tau_{nt}}{S_{23}^s}\right)^2 + \left(\frac{\tau_{n1}}{S_{12}^s}\right)^2 + (K^-\sigma_n)^2} + K^-\sigma_n$ $K^- = \begin{cases} \frac{1}{\tau_{nt}^2 + \tau_{n1}^2}\left(\frac{P_{23}^-}{S_{23}^s}\tau_{nt}^2 + \frac{P_{13}^-}{S_{12}^s}\tau_{n1}^2\right) & \text{if } \tau_{nt}^2 + \tau_{n1}^2 > 0 \\ 0 & \text{if } \tau_{nt}^2 + \tau_{n1}^2 = 0 \end{cases}$

Table 7. Interactive failure criteria associated with failure modes.

In Puck's failure criterion, $\sigma_n, \tau_{n1}, \tau_{n2}$ correspond to the stresses on the action plane parallel to the fibres. The Puck constants, $P_{13}^+ = 0.35$, $P_{13}^- = 0.3$, $P_{23}^+ = 0.25$, $P_{23}^- = 0.2$, that correspond to the tensile and compressive inclination parameters, were defined according to the recommendations given in [60].

References

[1] Mattsson D, Joffe R, Varna J. Methodology for characterization of internal structure parameters governing performance in NCF composites. Composites Part B: Engineering. 2007;38:44-57.

[2] Drapier S, Wisnom M. Finite-element investigation of the compressive strength of non-crimp-fabric-based composites. Composites Science and Technology. 1999;59:1287-97.

[3] Dransfield K, Baillie C, Mai Y-W. Improving the delamination resistance of CFRP by stitching—a review. Composites Science and Technology. 1994;50:305-17.
[4] Miller AJ. The effect of microstructural parameters on the mechanical properties of non-crimp fabric composites: Cranfield University, School of Industrial and Manufacturing Science, 1996.
[5] Drapier S, Wisnom M. A finite-element investigation of the interlaminar shear behaviour of non-crimp-fabric-based composites. Composites Science and Technology. 1999;59:2351-62.
[6] González A, Graciani E, París F. Prediction of in-plane stiffness properties of non-crimp fabric laminates by means of 3D finite element analysis. Composites Science and Technology. 2008;68:121-31.
[7] Marklund E, Asp LE. Multiscale methodology for matrix failure prediction in non-crimp fabric composites. 14th European Conference on Composite Materials. Budapest, Hungary2010.
[8] Mattsson D, Joffe R, Varna J. Damage in NCF composites under tension: Effect of layer stacking sequence. Engineering Fracture Mechanics. 2008;75:2666-82.
[9] Mattsson HD, Varna J. Average Strain in Fiber Bundles and Its Effect on NCF Composite Stiffness. Journal of Engineering Materials and Technology. 2006;129:211-9.
[10] Lomov S, Ivanov D, Verpoest I, Zako M, Kurashiki T, Nakai H, et al. Meso-FE modelling of textile composites: Road map, data flow and algorithms. Composites Science and Technology. 2007;67:1870-91.
[11] Lomov SV, Verpoest I. Modelling of the internal structure and deformability of textile reinforcements: WiseTex software. Composites for the Future, 10th European Conference on Composite Materials (ECCM-10). Brugge, Belgium2002.
[12] Kurashiki T, Watanabe Y, Fujita Y, Watanabe Y, Zako M. Estimation of the mechanical behaviors for textile composites based on multi-scale analysis. ICCM 18 - The 18th International Conference on Composite Materials. ICC Jeju, Korea2011.
[13] Kurashiki T, Watanabe Y, Matsushima Y, Zako M, Lomov S, Verpoest I. Effects of stitching parameters on damage development for non-crimp fabric composites under tensile loading. ECCM15 - 15th European Conference on Composite Materials. Venice, Italy2012.
[14] Yan S, Zeng X, Long A. Meso-scale modelling of 3D woven composite T-joints with weave variations. Composites Science and Technology. 2019;171:171-9.
[15] Robitaille F, Clayton BR, Long AC, Souter BJ, Rudd CD. Geometric modelling of industrial preforms: Woven and braided textiles. Proceedings of the Institution of Mechanical Engineers, Part L: Journal of Materials: Design and Applications. 1999;213:69-83.
[16] Robitaille F, Clayton BR, Long AC, Souter BJ, Rudd CD. Geometric modelling of industrial preforms: Warp-knitted textiles. Proceedings of the Institution of Mechanical Engineers, Part L: Journal of Materials: Design and Applications. 2000;214:71-90.
[17] Topal S, Baiocchi L, Crocombe AD, Ogin SL, Potluri P, Withers PJ, et al. Late-stage fatigue damage in a 3D orthogonal non-crimp woven composite: An experimental and numerical study. Composites Part A: Applied Science and Manufacturing. 2015;79:155-63.
[18] Hinton MJ, Soden PD. Predicting failure in composite laminates: the background to the exercise. Composites Science and Technology. 1998;58:1001-10.
[19] Hinton MJ, Kaddour AS, Soden PD. A further assessment of the predictive capabilities of current failure theories for composite laminates: comparison with experimental evidence. Composites Science and Technology. 2004;64:549-88.
[20] Kachanov L. Time of the Rupture Process under Creep Conditions. Izvestiia Akademii Nauk SSSR, Otdelenie Teckhnicheskikh Nauk. 1958;8:26-31.
[21] Lemaitre J. A Course on Damage Mechanics. 1 ed: Springer-Verlag Berlin Heidelberg, 1992.

[22] Lemaitre J, Chaboche J-L. Mechanics of Solid Materials: Cambridge University Press, 1990.
[23] Chaboche J-L. Continuous damage mechanics — A tool to describe phenomena before crack initiation. Nuclear Engineering and Design. 1981;64:233-47.
[24] Matzenmiller A, Lubliner J, Taylor RL. A constitutive model for anisotropic damage in fiber-composites. Mechanics of Materials. 1995;20:125-52.
[25] Hashin Z. Failure Criteria for Unidirectional Fiber Composites. Journal of Applied Mechanics. 1980;47:329-34.
[26] Maimí P, Camanho PP, Mayugo JA, Dávila CG. A continuum damage model for composite laminates: Part I – Constitutive model. Mechanics of Materials. 2007;39:897-908.
[27] Maimí P, Camanho PP, Mayugo JA, Dávila CG. A continuum damage model for composite laminates: Part II – Computational implementation and validation. Mechanics of Materials. 2007;39:909-19.
[28] Barbero EJ, de Vivo L. A Constitutive Model for Elastic Damage in Fiber-Reinforced PMC Laminae. International Journal of Damage Mechanics. 2001;10:73-93.
[29] Schipperen JHA. An anisotropic damage model for the description of transverse matrix cracking in a graphite–epoxy laminate. Composite Structures. 2001;53:295-9.
[30] Liu PF, Zheng JY. Progressive failure analysis of carbon fiber/epoxy composite laminates using continuum damage mechanics. Materials Science and Engineering: A. 2008;485:711-7.
[31] Lapczyk I, Hurtado JA. Progressive damage modeling in fiber-reinforced materials. Composites Part A: Applied Science and Manufacturing. 2007;38:2333-41.
[32] Fakoor M, Mohammad Navid Ghoreishi S. Experimental and numerical investigation of progressive damage in composite laminates based on continuum damage mechanics. Polymer Testing. 2018;70:533-43.
[33] Cairns DS, Nelson JW, Woo K, Miller D. Progressive damage analysis and testing of composite laminates with fiber waves. Composites Part A: Applied Science and Manufacturing. 2016;90:51-61.
[34] Barbero EJ, Shahbazi M. Determination of material properties for ANSYS progressive damage analysis of laminated composites. Composite Structures. 2017;176:768-79.
[35] Eliopoulos EN, Kostopoulos V, Philippidis TP. A three-dimensional progressive damage FE model for GFRP composites under monotonic loading. Composites Science and Technology. 2016;123:79-91.
[36] ANSYS. 18 ed. 2018.
[37] Ferreira LM, Graciani E, París F. Modelling the waviness of the fibres in non-crimp fabric composites using 3D finite element models with straight tows. Composite Structures. 2014;107:79-87.
[38] Ferreira LM, Graciani E, París F. Three dimensional finite element study of the behaviour and failure mechanism of non-crimp fabric composites under in-plane compression. Composite Structures. 2016;149:106-13.
[39] Ferreira LM, Graciani E, París F. Progressive damage study of NCF composites under compressive loading. ECCM16 - 16th European Conference on Composite Materials. Seville, Spain2014. p. 56.
[40] Puck A, Schürmann H. Failure analysis of FRP laminates by means of physically based phenomenological models. Composites Science and Technology. 2002;62:1633-62.
[41] Sinclar R, Robinson P, Iannucci L. Directed compression tests on FALCOM biaxial cross-ply material. FALCOM/WP3/ICL/TR01. Imperial College London; 2005.
[42] Chamis C. Mechanics of Composite Materials: Past, Present, and Future. National Aeronautics and Space Administration; 1984. p. 41.

[43] Green SD, Matveev MY, Long AC, Ivanov D, Hallett SR. Mechanical modelling of 3D woven composites considering realistic unit cell geometry. Composite Structures. 2014;118:284-93.
[44] Lomov SV, Ivanov DS, Verpoest I, Zako M, Kurashiki T, Nakai H, et al. Meso-FE modelling of textile composites: Road map, data flow and algorithms. Composites Science and Technology. 2007;67:1870-91.
[45] Xu J, Lomov SV, Verpoest I, Daggumati S, Paepegem WV, Degrieck J, et al. A progressive damage model of textile composites on meso-scale using finite element method: static damage analysis. Journal of Composite Materials. 2014;48:3091-109.
[46] HEXCEL. HexPly M36 Product data sheet. 2019.
[47] TohoTenax America Inc. HTS40 data sheet. 2008.
[48] Mattsson D, Joffe R, Varna J. Characterisation of processability and manufacturing. Characterisation of microstructure. FALCOM/WP2:D2.1-4/LTU. 2004.
[49] Longitudinal Shear Modulus of Single Aramid, Carbon and Glass Fibres by Torsion Pendulum Tests. International Journal of Mechanical, Aerospace, Industrial, Mechatronic and Manufacturing Engineering. 2014;8:422-8.
[50] Villeneuve JF, Naslain R. Shear moduli of carbon, Si-C-O, Si-C-Ti-O and alumina single ceramic fibers as assessed by torsion pendulum tests. Composites Science and Technology. 1993;49:191-203.
[51] Maurin R, Davies P, Baral N, Baley C. Transverse Properties of Carbon Fibres by Nano-Indentation and Micro-mechanics. Applied Composite Materials. 2008;15:61-73.
[52] Miyagawa H, Mase T, Sato C, Drown E, Drzal LT, Ikegami K. Comparison of experimental and theoretical transverse elastic modulus of carbon fibers. Carbon. 2006;44:2002-8.
[53] Herakovich CT. Mechanics of Fibrous Composites: John Wiley and Sons, 1997.
[54] Asp LE, Öhgren I, Holmberg JA. Determination of fibre content on RFI plates for G1c and OHT testing. FALCOM/WP3/SI/TECH001. 2004.
[55] Lubin G. Handbook of composites. Second ed: Chapman & Hall, 1998.
[56] Creemers RJC. Interlaminar shear strength criteria for composites - An assessment by means of statistical analysis. National Aerospace Laboratory NLR; 2010.
[57] Sun CT, Quinn BJ, Tao J, Oplinger DW. Comparative evaluation of failure analysis methods for composite laminates. Washington, D.C. 20591: U.S. Department of Transportation - Federal Aviation Administration; 1996. p. 132.
[58] Ferreira LM. Study of the behaviour of non-crimp fabric laminates by 3D finite element models. PhD. Thesis. Sevilla: University of Seville, 2012.
[59] Joffe R, Mattsson D, Modniks J, Varna J. Compressive failure analysis of non-crimp fabric composites with large out-of-plane misalignment of fiber bundles. Composites Part a-Applied Science and Manufacturing. 2005;36:1030-46.
[60] Puck A, Kopp J, Knops M. Guidelines for the determination of the parameters in Puck's action plane strength criterion. Composites Science and Technology. 2002;62:371-8.